

# Riemannian Preconditioned Algorithms for Tensor Completion via Tensor Ring Decomposition\*

Bin Gao<sup>†</sup>, Renfeng Peng<sup>‡</sup>, and Ya-xiang Yuan<sup>†</sup>

**Abstract.** We propose Riemannian preconditioned algorithms for the tensor completion problem via tensor ring decomposition. A new Riemannian metric is developed on the product space of the mode-2 unfolding matrices of the core tensors in tensor ring decomposition. The construction of this metric aims to approximate the Hessian of the cost function by its diagonal blocks, paving the way for various Riemannian optimization methods. Specifically, we propose the Riemannian gradient descent and Riemannian conjugate gradient algorithms. We prove that both algorithms globally converge to a stationary point. In the implementation, we exploit the tensor structure and design an economical procedure to avoid large matrix formulation and computation in gradients, which significantly reduces the computational cost. Numerical experiments on various synthetic and real-world datasets—movie ratings, hyperspectral images, and high-dimensional functions—suggest that the proposed algorithms are more efficient and have better reconstruction ability than other candidates.

**Key words.** Tensor completion, tensor ring decomposition, Riemannian optimization, preconditioned gradient

**AMS subject classifications.** 15A69, 58C05, 65K05, 90C30

**1. Introduction.** The tensor completion problem, as a natural generalization of the matrix completion problem, is a task of recovering a tensor based on its partially observed entries. In practice, datasets collected from real applications are often assumed to have underlying low-rank structure. Therefore, low-rank matrix decompositions are widely used in matrix completion, which can save the computational cost and storage. In the same spirit, low-rank tensor decompositions play a significant role in tensor completion; applications can be found across various fields, e.g., recommendation systems [19, 12], image processing [24], and interpolation of high-dimensional functions [32, 21].

In this paper, we consider tensor ring decomposition and focus on the following tensor completion problem with bounded tensor ring rank  $\mathbf{r} := (r_1, \dots, r_d)$ . Given a partially observed tensor  $\mathcal{A} \in \mathbb{R}^{n_1 \times \dots \times n_d}$  on an index set  $\Omega \subseteq [n_1] \times \dots \times [n_d]$ , where  $[n_k] := \{1, 2, \dots, n_k\}$  for  $k = 1, \dots, d$ . The tensor completion problem is formulated as follows,

$$(1.1) \quad \begin{aligned} \min_{\mathcal{X} \in \mathbb{R}^{n_1 \times \dots \times n_d}} \quad & \frac{1}{2} \|\mathbb{P}_\Omega(\mathcal{X}) - \mathbb{P}_\Omega(\mathcal{A})\|_F^2 \\ \text{s. t.} \quad & \mathcal{X} = \llbracket \mathcal{U}_1, \dots, \mathcal{U}_d \rrbracket, \end{aligned}$$

where  $\llbracket \mathcal{U}_1, \dots, \mathcal{U}_d \rrbracket$  denotes the tensor ring decomposition of  $\mathcal{X} \in \mathbb{R}^{n_1 \times \dots \times n_d}$  with core tensors  $\mathcal{U}_k \in \mathbb{R}^{r_k \times n_k \times r_{k+1}}$  for  $k \in [d]$ ; see definitions in [section 2](#).  $\mathbb{P}_\Omega$  denotes the projec-

\*Submitted to the editors February 28, 2023.

**Funding:** This work was funded by the National Natural Science Foundation of China (grant No.12288201).

<sup>†</sup>State Key Laboratory of Scientific and Engineering Computing, Academy of Mathematics and Systems Science, Chinese Academy of Sciences, China ({gaobin, yx}@lsec.cc.ac.cn).

<sup>‡</sup>Corresponding author. State Key Laboratory of Scientific and Engineering Computing, Academy of Mathematics and Systems Science, Chinese Academy of Sciences, and University of Chinese Academy of Sciences, China (pengrenfeng@lsec.cc.ac.cn).

tion operator onto  $\Omega$ , namely,  $P_\Omega(\mathcal{X})(i_1, \dots, i_d) = \mathcal{X}(i_1, \dots, i_d)$  if  $(i_1, \dots, i_d) \in \Omega$ , otherwise  $P_\Omega(\mathcal{X})(i_1, \dots, i_d) = 0$ .

*Related works and motivation.* Tensor completion has several different formulations, one type is based on the nuclear norm minimization. In matrix completion, the nuclear norm of a matrix—a convex relaxation of matrix rank—is minimized. Liu et al. [24] extended the “nuclear norm” to tensor by calculating the sum of nuclear norms of unfolding matrices of a tensor, and applied the alternating direction method of multipliers algorithm to solve the tensor completion problem. Since the tensor data observed in real world may be perturbed by noise, Zhao et al. [38] focused on the robust tensor completion problem based on the tubal nuclear norm, and proposed a proximal majorization-minimization algorithm. These algorithms require storing tensors in full size, and the number of parameters is  $n_1 \cdots n_d$ , which scales exponentially to the dimension  $d$ .

Instead of working with full-size tensors, tensor decompositions [22] allow us to take advantage of the low-rank structure in tensor completion problems, and thus can reduce the number of parameters in search space and save storage. In view of the block structure in tensor decompositions, one can develop alternating minimization methods by updating one block while fixing others. Jain and Oh [18] proposed an alternating minimization method for symmetric third order tensors in canonical polyadic (CP) decomposition. For Tucker decomposition, the alternating minimization, also called the alternating least squares (ALS) algorithm, was considered by Andersson and Bro [3] in which the subproblem is a least squares problem. Tensor train (TT) decomposition [26, 27], also known as matrix product states [33, 29] in computational physics, decomposes a tensor into  $d$  core tensors. Grasedyck et al. [15] presented an alternating direction fitting algorithm for the tensor completion problem. Recently, tensor ring (TR) decomposition was proposed by Zhao et al. [37] as a generalization of tensor train decomposition. Compared to TT decomposition, TR decomposition relaxes the rank constraint on the first and last core in TT from one to an arbitrary interger, i.e., from TT rank  $(1, r_2, \dots, r_d, 1)$  to TR rank  $(r_1, r_2, \dots, r_d)$ , providing higher compressibility and flexibility [36]. The ALS algorithm was developed to solve the TR decomposition problem in [37], and it was further applied to tensor completion [34]. In general, ALS methods in which the number of parameters scales linearly to the dimension  $d$  have been proved to be effective for the tensor completion problem. However, they may suffer from overfitting and require careful initialization in practice [11].

More recently, Riemannian optimization working with tensor-based manifolds appears to be prosperous for solving completion problems. Since the search space is a manifold, one can benefit from different geometric tools and develop efficient optimization methods on the manifold that have convergence results; see [1, 6] for an overview. Acar et al. [2] proposed an Euclidean nonlinear conjugate gradient method for tensor completion via CP decomposition. Dong et al. [12] proposed Riemannian gradient and Riemannian conjugate gradient methods based on a Riemannian metric on the product space of matrices in polyadic decomposition. For tensor completion in Tucker decomposition, Kressner et al. [23] proposed a Riemannian conjugate gradient method on the manifold of rank-constrained tensors. Kasai and Mishra [19] introduced a preconditioned metric and considered the quotient geometry of the manifold via Tucker decomposition. The corresponding Riemannian conjugate gradient algorithm was proposed. Based on geometric properties of the manifold of tensors with fixed TT rank,

Steinlechner [32] proposed a Riemannian conjugate gradient algorithm. Furthermore, Cai et al. [9] investigated the quotient geometry on this manifold, and proposed Riemannian gradient, Riemannian conjugate gradient and Riemannian Gauss–Newton algorithms.

As a generalization of TT decomposition, on the one hand, tensor ring decomposition provides a flexible choice of tensor rank. Specifically, the unfolding matrices of core tensors in TR are not necessarily to be of full rank while the mode-1 and mode-3 unfolding matrices of core tensors in TT have to be of full rank. It implies that TR-based algorithms tolerate the rank-deficient factor matrices, which is favorable in practice. On the other hand, TR decomposition preserves a similar block structure as TT. Hence, it allows us to endow the search space with a manifold structure and to develop a preconditioned metric. In this paper, we are interested in Riemannian optimization methods on the search space

$$\mathcal{M} = \mathbb{R}^{n_1 \times r_1 r_2} \times \mathbb{R}^{n_2 \times r_2 r_3} \times \dots \times \mathbb{R}^{n_{d-1} \times r_{d-1} r_d} \times \mathbb{R}^{n_d \times r_d r_1}$$

for the tensor completion problem via TR decomposition.

**Contributions.** We formulate the tensor completion problem via tensor ring decomposition, in which the search space is a product space of the mode-2 unfolding matrices of the core tensors in tensor ring decomposition. We design a *preconditioned* metric on the search space, and propose the Riemannian gradient descent and Riemannian conjugate gradient algorithms to solve the tensor completion problem. We prove that every accumulation point of the sequence generated by the proposed algorithms is a stationary point. To the best of our knowledge, this is the first Riemannian formulation of the tensor completion problem in TR decomposition.

The computation of (Riemannian) gradients involves large matrix formulation and multiplication. Its computational cost is exponential to the dimension  $d$ , which is unaffordable in practice. In order to improve the efficiency of the proposed algorithms, we design an economical procedure, which has polynomial complexity to the dimension  $d$ , to compute the (Riemannian) gradients by exploiting the tensor structure in TR.

We compare the proposed algorithms with existing methods in various tensor completion tasks on both synthetic and real-world datasets, including movie ratings, hyperspectral images, and high-dimensional functions. The numerical results illustrate that the TR-based algorithms have better or comparable recovery performance than the others. In addition, the proposed algorithms are more efficient than the alternating least squares among TR-based algorithms.

**Organization.** First, the preliminaries of tensor ring decomposition and the tensor completion problem are introduced in [section 2](#). Next, we develop Riemannian algorithms and present computational details in [section 3](#). The convergence results of the proposed algorithms are shown in [section 4](#). Numerical results are reported in [section 5](#). Finally, the conclusion is given in [section 6](#).

**2. Preliminaries.** In this section, we first introduce the notation in tensor operations and the definition of tensor ring decomposition. Next, a formulation of the TR-based tensor completion problem (1.1) is described.

The following notions are involved in tensor computations [22]. The mode- $k$  unfolding of a tensor  $\mathcal{X} \in \mathbb{R}^{n_1 \times \dots \times n_d}$  is denoted by a matrix  $\mathbf{X}_{(k)} \in \mathbb{R}^{n_k \times n_{-k}}$ , where  $n_{-k} := \prod_{i \neq k} n_i$ . The  $(i_1, i_2, \dots, i_d)$ -th entry of  $\mathcal{X}$  corresponds to the  $(i_k, j)$ -th entry of  $\mathbf{X}_{(k)}$ , where

$j = 1 + \sum_{\ell \neq k, \ell=1}^d (i_\ell - 1) J_\ell$  with  $J_\ell = \prod_{m=1, m \neq k}^{\ell-1} n_m$ , for  $k = 1, \dots, d$ . We define an index mapping  $\pi_k$  by  $\pi_k : (i_1, \dots, i_{k-1}, i_{k+1}, \dots, i_d) \mapsto j$ . Similarly, the mode- $k$  unfolding of indexes in a sampling set  $\Omega$  is defined by  $\Omega_{(k)} := \{(i_k, j) : (i_1, \dots, i_d) \in \Omega\}$ . The inverse of the mode- $k$  unfolding operator  $(\cdot)_{(k)}$  is called the  $k$ -th tensorization operator, denoted by  $\text{ten}_{(k)}(\cdot)$ . The inner product between two tensors  $\mathcal{X}, \mathcal{Y} \in \mathbb{R}^{n_1 \times \dots \times n_d}$  is defined by  $\langle \mathcal{X}, \mathcal{Y} \rangle := \sum_{i_1=1}^{n_1} \dots \sum_{i_d=1}^{n_d} \mathcal{X}(i_1, \dots, i_d) \mathcal{Y}(i_1, \dots, i_d)$ . The Frobenius norm of a tensor  $\mathcal{X}$  is defined by  $\|\mathcal{X}\|_F := \sqrt{\langle \mathcal{X}, \mathcal{X} \rangle}$ .

**Definition 2.1 (tensor ring decomposition [37]).** Given a  $d$ -th order tensor  $\mathcal{X} \in \mathbb{R}^{n_1 \times \dots \times n_d}$ , tensor ring decomposition, denoted by

$$\mathcal{X} = \llbracket \mathcal{U}_1, \dots, \mathcal{U}_d \rrbracket,$$

decomposes  $\mathcal{X}$  into  $d$  core tensors  $\mathcal{U}_k \in \mathbb{R}^{r_k \times n_k \times r_{k+1}}$  for  $k = 1, \dots, d$  and  $r_{d+1} = r_1$ . Specifically, the  $(i_1, \dots, i_d)$ -th entry of  $\mathcal{X}$  is represented by the trace of products of  $d$  matrices, i.e.,

$$\mathcal{X}(i_1, \dots, i_d) = \text{tr}(\mathbf{U}_1(i_1) \cdots \mathbf{U}_d(i_d)),$$

where  $\mathbf{U}_k(i_k) = \mathcal{U}_k(:, i_k, :) \in \mathbb{R}^{r_k \times r_{k+1}}$  is the lateral slice matrix of  $\mathcal{U}_k$  for  $i_k = 1, \dots, n_k$ .

The tuple  $\mathbf{r} = (r_1, \dots, r_d)$  is referred to as the tensor ring rank (TR rank). Figure 1 illustrates the TR decomposition of a tensor.

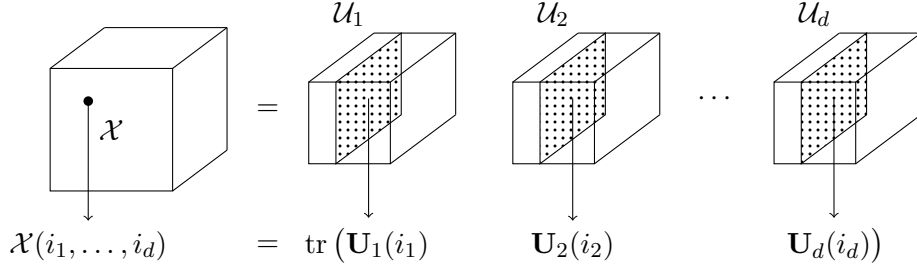


**Figure 1.** Illustration of tensor ring decomposition of a tensor.

In view of the cyclic symmetry of trace operator, we rewrite the  $(i_1, \dots, i_d)$ -th entry of tensor  $\mathcal{X}$  in tensor ring decomposition as follows,

$$\begin{aligned} \text{tr}(\mathbf{U}_1(i_1) \cdots \mathbf{U}_d(i_d)) &= \text{tr}(\mathbf{U}_k(i_k) \mathbf{U}_{k+1}(i_{k+1}) \cdots \mathbf{U}_d(i_d) \mathbf{U}_1(i_1) \cdots \mathbf{U}_{k-1}(i_{k-1})) \\ &= \langle \text{vec}(\mathbf{U}_k(i_k)), \text{vec}((\mathbf{U}_{k+1}(i_{k+1}) \cdots \mathbf{U}_d(i_d) \mathbf{U}_1(i_1) \cdots \mathbf{U}_{k-1}(i_{k-1}))^\top) \rangle, \end{aligned}$$

where  $\text{vec}(\cdot)$  denotes the column vectorization of a matrix.  $\text{vec}(\mathbf{U}_k(i_k))^\top$  is the  $i_k$ -th row of the mode-2 unfolding matrix  $(\mathcal{U}_k)_{(2)} \in \mathbb{R}^{n_k \times r_k r_{k+1}}$  of the core tensor  $\mathcal{U}_k$ . We intend to define a tensor  $\mathcal{U}_{\neq k}$  such that the  $\pi_k(i_1, \dots, i_{k-1}, i_{k+1}, \dots, i_d)$ -th row of the mode-2 unfolding matrix  $(\mathcal{U}_{\neq k})_{(2)}$  is the second term in the above inner product.

**Definition 2.2 (subchain tensor).** The subchain tensor  $\mathcal{U}_{\neq k} \in \mathbb{R}^{r_k \times \prod_{j \neq k} n_j \times r_{k+1}}$  is defined by its lateral slice matrices, i.e.,

$$(2.1) \quad \mathbf{U}_{\neq k}(\pi_k(i_1, \dots, i_{k-1}, i_{k+1}, \dots, i_d)) := (\mathbf{U}_{k+1}(i_{k+1}) \cdots \mathbf{U}_d(i_d) \mathbf{U}_1(i_1) \cdots \mathbf{U}_{k-1}(i_{k-1}))^\top.$$

Given the mode-2 unfolding matrix  $(\mathcal{U}_k)_{(2)}$  and subchain tensor in [Definition 2.2](#), the mode- $k$  unfolding of a tensor  $\mathcal{X}$  in tensor ring decomposition equals to the product of two smaller matrices (see [\[37, Theorem 3.5\]](#)), i.e.,

$$\mathbf{X}_{(k)} = \mathbf{W}_k \mathbf{W}_{\neq k}^\top,$$

where  $\mathbf{W}_k := (\mathcal{U}_k)_{(2)} \in \mathbb{R}^{n_k \times r_k r_{k+1}}$  and  $\mathbf{W}_{\neq k} := (\mathcal{U}_{\neq k})_{(2)} \in \mathbb{R}^{n_{-k} \times r_k r_{k+1}}$  for  $k = 1, \dots, d$ . Subsequently, the tensor completion problem [\(1.1\)](#) can be reformulated on the product space of the mode-2 unfolding matrices of the core tensors in TR decomposition

$$\mathcal{M} := \mathbb{R}^{n_1 \times r_1 r_2} \times \mathbb{R}^{n_2 \times r_2 r_3} \times \dots \times \mathbb{R}^{n_{d-1} \times r_{d-1} r_d} \times \mathbb{R}^{n_d \times r_d r_1}.$$

The Frobenius norm on  $\mathcal{M}$  is defined by  $\|\vec{\mathbf{W}}\|_F = \sqrt{\sum_{k=1}^d \|\mathbf{W}_k\|_F^2}$  for  $\vec{\mathbf{W}} = (\mathbf{W}_1, \dots, \mathbf{W}_d) \in \mathcal{M}$ .

In this paper, we focus on the following tensor completion problem combined with a sample set  $\Omega$  and a regularization term  $r$ ,

$$(2.2) \quad \min_{\vec{\mathbf{W}}=(\mathbf{W}_1, \dots, \mathbf{W}_d) \in \mathcal{M}} f(\vec{\mathbf{W}}) := f_\Omega(\vec{\mathbf{W}}) + r(\vec{\mathbf{W}}).$$

The objective function  $f$  consists of two parts: one is the cost function

$$f_\Omega(\vec{\mathbf{W}}) := \frac{1}{2p} \|\mathbb{P}_\Omega(\mathcal{X}) - \mathbb{P}_\Omega(\mathcal{A})\|_F^2 = \frac{1}{2p} \left\| \mathbb{P}_{\Omega_{(k)}} \left( \mathbf{W}_k \mathbf{W}_{\neq k}^\top \right) - \mathbb{P}_{\Omega_{(k)}} \left( \mathbf{A}_{(k)} \right) \right\|_F^2,$$

where  $p := \frac{|\Omega|}{n_1 \dots n_d}$  is the *sampling rate*,  $\mathbf{A}_{(k)}$  denotes the mode- $k$  unfolding matrix of  $\mathcal{A}$ , and  $\Omega_{(k)}$  is the mode- $k$  unfolding of the sample set  $\Omega$ ; the other is a regularization term  $r(\vec{\mathbf{W}})$  and we choose

$$r(\vec{\mathbf{W}}) := \frac{\lambda}{2} \|\vec{\mathbf{W}}\|_F^2$$

in a similar fashion as Maximum-margin Matrix Factorization [\[31\]](#) with  $\lambda > 0$ . The regularization term keeps the variable  $\vec{\mathbf{W}}$  in a compact subset of  $\mathcal{M}$  and guarantees the convergence; see analysis in [section 4](#).

Note that an element  $\vec{\mathbf{W}} = (\mathbf{W}_1, \dots, \mathbf{W}_d)$  in the product of matrix space  $\mathcal{M}$  can also represent an element  $\llbracket \text{ten}_{(2)}(\mathbf{W}_1), \dots, \text{ten}_{(2)}(\mathbf{W}_d) \rrbracket$  in TR decomposition, where  $\text{ten}_{(2)}(\cdot)$  is the second tensorization operator. Since  $\text{ten}_{(2)}(\cdot)$  is an invertible operator, the mapping

$$(2.3) \quad \tau : \mathcal{M} \rightarrow \mathbb{R}^{n_1 \times \dots \times n_d}, \quad \tau(\vec{\mathbf{W}}) := \llbracket \text{ten}_{(2)}(\mathbf{W}_1), \dots, \text{ten}_{(2)}(\mathbf{W}_d) \rrbracket$$

is bijective. It turns out that the search space in [\(2.2\)](#) is equivalent to the one in the original problem [\(1.1\)](#). Moreover, we adopt [\(2.3\)](#) as the generation of synthetic data in [section 5](#).

Given the objective function  $f$ , the first-order derivative with respect to  $\mathbf{W}_k$  has the following form,

$$\partial_{\mathbf{W}_k} f(\vec{\mathbf{W}}) = \partial_{\mathbf{W}_k} f_\Omega(\vec{\mathbf{W}}) + \partial_{\mathbf{W}_k} r(\vec{\mathbf{W}}) = \frac{1}{p} \mathbf{S}_{(k)} \mathbf{W}_{\neq k} + \lambda \mathbf{W}_k \quad \text{for } k = 1, \dots, d,$$

where  $\mathcal{S} := P_\Omega(\tau(\vec{\mathbf{W}})) - P_\Omega(\mathcal{A})$  is called the residual tensor and  $\mathbf{S}_{(k)}$  is the mode- $k$  unfolding matrix of tensor  $\mathcal{S}$ . Therefore, the Euclidean gradient of  $f_\Omega$  at  $\vec{\mathbf{W}} \in \mathcal{M}$  can be computed as follows,

$$(2.4) \quad \nabla f_\Omega(\vec{\mathbf{W}}) = \left( \frac{1}{p} \mathbf{S}_{(1)} \mathbf{W}_{\neq 1} + \lambda \mathbf{W}_1, \dots, \frac{1}{p} \mathbf{S}_{(d)} \mathbf{W}_{\neq d} + \lambda \mathbf{W}_d \right).$$

Moreover, one can develop Euclidean gradient descent algorithms (e.g., [35]) to solve the completion problem (2.2). Recently, Riemannian preconditioned algorithms are considered in which the search space is endowed with a non-Euclidean metric. The construction of this metric aims to approximate the Hessian of the cost function by its ‘‘diagonal blocks’’. These algorithms improve the performance of Euclidean-based algorithms, and are successfully applied to matrix and tensor completion (e.g., [25, 19, 12, 9]). However, the extension to TR is not straightforward since it involves large matrix computation and formulation. In next section, we consider how to develop efficient preconditioned algorithms for the tensor completion problem (2.2).

**3. Tensor completion algorithms.** We first develop a preconditioned metric on the manifold  $\mathcal{M}$ . The corresponding Riemannian gradient is derived under this metric. Next, we propose the Riemannian gradient descent and Riemannian conjugate gradient algorithms. An efficient procedure for computing the Riemannian gradient is proposed in the end.

**3.1. A preconditioned metric.** The idea of a preconditioned metric on  $\mathcal{M}$  is to take advantage of the second-order information of the cost function  $f_\Omega$  and to formulate a search direction that approximates the Newton direction. Specifically, we intend to construct an operator  $\mathcal{H}(\vec{\mathbf{W}}) : T_{\vec{\mathbf{W}}} \mathcal{M} \rightarrow T_{\vec{\mathbf{W}}} \mathcal{M}$  such that

$$(3.1) \quad \langle \mathcal{H}(\vec{\mathbf{W}})[\vec{\xi}], \vec{\eta} \rangle \approx \nabla^2 f_\Omega(\vec{\mathbf{W}})[\vec{\xi}, \vec{\eta}]$$

for all  $\vec{\xi}, \vec{\eta} \in T_{\vec{\mathbf{W}}} \mathcal{M}$ , where  $T_{\vec{\mathbf{W}}} \mathcal{M}$  denotes the tangent space to  $\mathcal{M}$  at  $\vec{\mathbf{W}}$  and  $\nabla^2 f_\Omega$  denotes the (Euclidean) Hessian of  $f_\Omega$ . Note that  $T_{\vec{\mathbf{W}}} \mathcal{M} = \mathbb{R}^{n_1 \times r_1 r_2} \times \dots \times \mathbb{R}^{n_{d-1} \times r_{d-1} r_d} \times \mathbb{R}^{n_d \times r_d r_1}$ .

To this end, we start from computing the explicit form of the Hessian operator

$$\nabla^2 f_\Omega(\vec{\mathbf{W}})[\vec{\xi}, \vec{\eta}] = \sum_{k=1}^d \langle \partial_{\mathbf{W}_k, \mathbf{W}_k}^2 f_\Omega(\vec{\mathbf{W}})[\vec{\xi}], \vec{\eta} \rangle + \sum_{\ell, m=1, \ell \neq m}^d \langle \partial_{\mathbf{W}_\ell, \mathbf{W}_m}^2 f_\Omega(\vec{\mathbf{W}})[\vec{\xi}], \vec{\eta} \rangle$$

for all  $\vec{\xi}, \vec{\eta} \in T_{\vec{\mathbf{W}}} \mathcal{M}$ . By direct calculations, the ‘‘diagonal blocks’’ of  $\nabla^2 f_\Omega(\vec{\mathbf{W}})$  have the following forms,

$$(3.2) \quad \partial_{\mathbf{W}_k, \mathbf{W}_k}^2 f_\Omega(\vec{\mathbf{W}})[\vec{\xi}] = \frac{1}{p} P_{\Omega(k)} \left( \xi_k \mathbf{W}_{\neq k}^\top \right) \mathbf{W}_{\neq k} \quad \text{for } k = 1, \dots, d.$$

Since computing the ‘‘off-diagonal blocks’’  $\partial_{\mathbf{W}_\ell, \mathbf{W}_m}^2 f_\Omega(\vec{\mathbf{W}})$  is complicated, we consider only the ‘‘diagonal blocks’’ as a trade-off between accuracy and computational cost to form an operator  $\mathcal{H}(\vec{\mathbf{W}})$ .

Assuming  $\Omega$  to be generated by certain subsampling pattern, we design a metric that is irrelevant to a specific sampling set  $\Omega$  by taking expectation on (3.2). More accurately,

we suppose that the indexes in  $\Omega$  are i.i.d. samples from the Bernoulli distribution with probability  $p$ . We eliminate the projection operator  $P_\Omega$  by taking expectation on “diagonal blocks” over  $\Omega$ . Hence, we can define the operator  $\mathcal{H}(\vec{\mathbf{W}})$  by

$$(3.3) \quad \begin{aligned} \mathcal{H}(\vec{\mathbf{W}})[\vec{\xi}] &:= \left( \mathbb{E}_\Omega \left[ \partial_{\mathbf{W}_1, \mathbf{W}_1}^2 f_\Omega(\vec{\mathbf{W}})[\vec{\xi}] \right], \dots, \mathbb{E}_\Omega \left[ \partial_{\mathbf{W}_d, \mathbf{W}_d}^2 f_\Omega(\vec{\mathbf{W}})[\vec{\xi}] \right] \right) \\ &= \left( \xi_1 \mathbf{W}_{\neq 1}^\top \mathbf{W}_{\neq 1}, \dots, \xi_d \mathbf{W}_{\neq d}^\top \mathbf{W}_{\neq d} \right). \end{aligned}$$

Consequently, we define a new metric as follows.

**Definition 3.1 (preconditioned metric).**  $g$  is an inner product on  $\mathcal{M}$  defined by

$$(3.4) \quad g_{\vec{\mathbf{W}}}(\vec{\xi}, \vec{\eta}) := \sum_{k=1}^d \text{tr} \left( \xi_k \mathbf{H}_k(\vec{\mathbf{W}}) (\eta_k)^\top \right)$$

for all  $\vec{\mathbf{W}} \in \mathcal{M}$  and  $\vec{\xi}, \vec{\eta} \in T_{\vec{\mathbf{W}}} \mathcal{M}$ , where  $\mathbf{H}_k(\vec{\mathbf{W}}) \in \mathbb{R}^{r_k r_{k+1} \times r_k r_{k+1}}$  is a matrix defined by

$$\mathbf{H}_k(\vec{\mathbf{W}}) := \mathbf{W}_{\neq k}^\top \mathbf{W}_{\neq k} + \delta \mathbf{I}_{r_k r_{k+1}}$$

with a constant parameter  $\delta > 0$  and the identity matrix  $\mathbf{I}_{r_k r_{k+1}} \in \mathbb{R}^{r_k r_{k+1} \times r_k r_{k+1}}$ .

Since the matrix  $\mathbf{W}_{\neq k}^\top \mathbf{W}_{\neq k}$  is not necessarily positive definite, a shifting term  $\delta \mathbf{I}_{r_k r_{k+1}}$  is added to avoid singularity. Moreover,  $g$  is smooth on  $\mathcal{M}$ , and thus is a well-defined Riemannian metric on  $\mathcal{M}$ . It turns out that  $\mathcal{M}$  is a Riemannian manifold endowed with  $g$  and the norm of a tangent vector  $\vec{\xi} \in T_{\vec{\mathbf{W}}} \mathcal{M}$  can be defined by  $\|\vec{\xi}\|_{\vec{\mathbf{W}}} := \sqrt{g_{\vec{\mathbf{W}}}(\vec{\xi}, \vec{\xi})}$ . The Riemannian gradient [1, §3.6],  $\text{grad} f(\vec{\mathbf{W}})$ , is the unique element in  $T_{\vec{\mathbf{W}}} \mathcal{M}$  that satisfies  $g_{\vec{\mathbf{W}}}(\text{grad} f(\vec{\mathbf{W}}), \vec{\xi}) = Df(\vec{\mathbf{W}})[\vec{\xi}] := \langle \nabla f(\vec{\mathbf{W}}), \vec{\xi} \rangle$  for all  $\vec{\xi} \in T_{\vec{\mathbf{W}}} \mathcal{M}$ . Note that  $g_{\vec{\mathbf{W}}}(\vec{\xi}, \vec{\eta}) = \langle (\mathcal{H} + \delta \mathcal{I})(\vec{\mathbf{W}})[\vec{\xi}], \vec{\eta} \rangle$ , where  $\mathcal{I}(\vec{\mathbf{W}}) : T_{\vec{\mathbf{W}}} \mathcal{M} \rightarrow T_{\vec{\mathbf{W}}} \mathcal{M}$  is the identity operator. It follows that

$$\text{grad} f(\vec{\mathbf{W}}) = (\mathcal{H} + \delta \mathcal{I})^{-1}(\vec{\mathbf{W}})[\nabla f(\vec{\mathbf{W}})].$$

In view of (2.2) and (3.1),  $\text{grad} f$  is an approximation of the Newton direction of  $f$ . As a result, the metric (3.4) has a preconditioning effect on the Euclidean gradient. Therefore, we refer to the new metric (3.4) as a *preconditioned metric* on  $\mathcal{M}$ . In summary, the Riemannian gradient can be computed from (2.4) as follows.

**Proposition 3.2 (Riemannian gradient).** *The Riemannian gradient of  $f$  at  $\vec{\mathbf{W}} \in \mathcal{M}$  with respect to the metric  $g$  is*

$$(3.5) \quad \text{grad} f(\vec{\mathbf{W}}) = \left( \partial_{\mathbf{W}_1} f(\vec{\mathbf{W}}) \mathbf{H}_1^{-1}(\vec{\mathbf{W}}), \dots, \partial_{\mathbf{W}_d} f(\vec{\mathbf{W}}) \mathbf{H}_d^{-1}(\vec{\mathbf{W}}) \right).$$

**3.2. Riemannian preconditioned algorithms.** Using the preconditioned metric (3.4) and the Riemannian gradient (3.5), we propose the Riemannian gradient descent and Riemannian conjugate gradient algorithms to solve the tensor completion problem (2.2).

*Riemannian gradient descent.* The Riemannian gradient descent algorithm is listed in [Algorithm 3.1](#). Note that the retraction on the manifold  $\mathcal{M}$  is the identity map. For the selection of stepsize, we consider the following two strategies: 1) we adopt exact line search by solving the following optimization problem

$$(3.6) \quad s_{\text{exact}}^{(t)} := \arg \min_{s>0} h(s) = f(\vec{\mathbf{W}}^{(t)} + s\vec{\boldsymbol{\eta}}^{(t)}).$$

Since  $h$  is a polynomial of  $s$  with degree  $2d$ , the solution  $s_{\text{exact}}^{(t)}$  is the root of the polynomial  $h'(s)$  with  $2d - 1$  degree; 2) alternatively, we consider Armijo backtracking line search. Given the initial stepsize  $s_0^{(t)} > 0$ , find the smallest integer  $\ell$ , such that for  $s^{(t)} = \rho^\ell s_0^{(t)} > s_{\min}$ , the inequality

$$(3.7) \quad f(\vec{\mathbf{W}}^{(t)}) - f(\vec{\mathbf{W}}^{(t)} + s^{(t)}\vec{\boldsymbol{\eta}}^{(t)}) \geq -s^{(t)} a g_{\vec{\mathbf{W}}^{(t)}} \left( \text{grad} f(\vec{\mathbf{W}}^{(t)}), \vec{\boldsymbol{\eta}}^{(t)} \right)$$

holds, where  $\rho, a \in (0, 1)$ ,  $s_{\min} > 0$  are backtracking parameters. The Riemannian Barzilai–Borwein (RBB) stepsize [\[17\]](#), defined by

$$(3.8) \quad s_{\text{RBB1}}^{(t)} := \frac{\|\vec{\mathbf{Z}}^{(t-1)}\|_{\vec{\mathbf{W}}^{(t)}}^2}{|g_{\vec{\mathbf{W}}^{(t)}}(\vec{\mathbf{Z}}^{(t-1)}, \vec{\mathbf{Y}}^{(t-1)})|} \quad \text{or} \quad s_{\text{RBB2}}^{(t)} := \frac{|g_{\vec{\mathbf{W}}^{(t)}}(\vec{\mathbf{Z}}^{(t-1)}, \vec{\mathbf{Y}}^{(t-1)})|}{\|\vec{\mathbf{Y}}^{(t-1)}\|_{\vec{\mathbf{W}}^{(t)}}^2},$$

where  $\vec{\mathbf{Z}}^{(t-1)} := \vec{\mathbf{W}}^{(t)} - \vec{\mathbf{W}}^{(t-1)}$  and  $\vec{\mathbf{Y}}^{(t-1)} := \text{grad} f(\vec{\mathbf{W}}^{(t)}) - \text{grad} f(\vec{\mathbf{W}}^{(t-1)})$ , appears to be favorable in many applications. Therefore, we set RBB to be the initial stepsize  $s_0^{(t)}$ . It is worth noting that the first initial stepsize  $s_0^{(0)}$  can be generated by exact line search [\(3.6\)](#) in practice.

---

**Algorithm 3.1** Riemannian Gradient Descent (TR-RGD)

---

**Input:**  $f : \mathcal{M} \rightarrow \mathbb{R}$ ,  $\vec{\mathbf{W}}^{(0)} \in \mathcal{M}$ , tolerance  $\varepsilon > 0$ ,  $t = 0$ ; backtracking parameters  $\rho, a \in (0, 1)$ ,  $s_{\min} > 0$ .

- 1: **while** the stopping criteria are not satisfied **do**
- 2:   Compute search direction  $\vec{\boldsymbol{\eta}}^{(t)} = -\text{grad} f(\vec{\mathbf{W}}^{(t)})$ .
- 3:   Compute stepsize  $s^{(t)}$  by exact line search [\(3.6\)](#) or Armijo backtracking [\(3.7\)](#).
- 4:   Update  $\vec{\mathbf{W}}^{(t+1)} = \vec{\mathbf{W}}^{(t)} + s^{(t)}\vec{\boldsymbol{\eta}}^{(t)}$ ;  $t = t + 1$ .
- 5: **end while**

**Output:**  $\vec{\mathbf{W}}^{(t)} \in \mathcal{M}$ .

---

*Riemannian conjugate gradient.* The Riemannian conjugate gradient algorithm is given in [Algorithm 3.2](#). For CG parameter  $\beta^{(t)}$ , we consider the Riemannian version [\[8\]](#) of the modified Hestenes–Stiefel rule (HS+) [\[16\]](#)

$$(3.9) \quad \beta^{(t)} := \max \left\{ \frac{g_{\vec{\mathbf{W}}^{(t)}} \left( \text{grad} f(\vec{\mathbf{W}}^{(t)}) - \text{grad} f(\vec{\mathbf{W}}^{(t-1)}), \text{grad} f(\vec{\mathbf{W}}^{(t)}) \right)}{g_{\vec{\mathbf{W}}^{(t)}} \left( \text{grad} f(\vec{\mathbf{W}}^{(t)}) - \text{grad} f(\vec{\mathbf{W}}^{(t-1)}), \vec{\boldsymbol{\eta}}^{(t-1)} \right)}, 0 \right\}.$$

The stepsize in [Algorithm 3.2](#) is determined by Armijo backtracking line search [\(3.7\)](#).

---

**Algorithm 3.2** Riemannian Conjugate Gradient (TR-RCG)

---

**Input:**  $f : \mathcal{M} \rightarrow \mathbb{R}$ ,  $\vec{\mathbf{W}}^{(0)} \in \mathcal{M}$ , tolerance  $\varepsilon > 0$ ,  $t = 0$ ,  $\vec{\boldsymbol{\eta}}^{(-1)} = 0$ ; backtracking parameters  $\rho, a \in (0, 1)$ ,  $s_{\min} > 0$ .

- 1: **while** the stopping criteria are not satisfied **do**
- 2:   Compute search direction  $\vec{\boldsymbol{\eta}}^{(t)} = -\text{grad}f(\vec{\mathbf{W}}^{(t)}) + \beta^{(t)}\vec{\boldsymbol{\eta}}^{(t-1)}$  with CG parameter [\(3.9\)](#).
- 3:   Compute stepsize  $s^{(t)}$  by Armijo backtracking line search [\(3.7\)](#).
- 4:   Update  $\vec{\mathbf{W}}^{(t+1)} = \vec{\mathbf{W}}^{(t)} + s^{(t)}\vec{\boldsymbol{\eta}}^{(t)}$ ;  $t = t + 1$ .
- 5: **end while**

**Output:**  $\vec{\mathbf{W}}^{(t)} \in \mathcal{M}$ .

---

In both algorithms, the computation of Riemannian gradient, involving large matrix formulation and multiplication, dominates the total cost. Since this cost is exponential to  $d$ , a straightforward implementation is not affordable in practice. To this end, we have to come up with a procedure that can compute the Riemannian gradient efficiently.

**3.3. Efficient computation for gradients.** We investigate the computational details of the Riemannian gradient [\(3.5\)](#) in this subsection. Generally, the computation of  $\text{grad}f(\vec{\mathbf{W}}) = (\boldsymbol{\eta}_1, \dots, \boldsymbol{\eta}_d)$  involves two steps: the first is computing the Euclidean gradient  $\nabla f(\vec{\mathbf{W}}) = (\mathbf{G}_1, \dots, \mathbf{G}_d)$  in [\(2.4\)](#); the second is assembling the Riemannian gradient  $\text{grad}f(\vec{\mathbf{W}})$ , where

$$\begin{aligned} \mathbf{G}_k &:= \partial_{\mathbf{W}_k} f(\vec{\mathbf{W}}) = \frac{1}{p} \mathbf{S}_{(k)} \mathbf{W}_{\neq k} + \lambda \mathbf{W}_k, \\ \boldsymbol{\eta}_k &:= \mathbf{G}_k \mathbf{H}_k^{-1}(\vec{\mathbf{W}}) = \mathbf{G}_k (\mathbf{W}_{\neq k}^\top \mathbf{W}_{\neq k} + \delta \mathbf{I}_{r_k r_{k+1}})^{-1} \end{aligned}$$

for  $k = 1, \dots, d$ .

There are five operations in straightforward calculating the gradients: 1) form the matrix  $\mathbf{W}_{\neq k}$  for  $k = 1, \dots, d$ , which requires  $2 \sum_{k=1}^d n_{-k} R_k$  flops, where  $R_k := r_k \left( \sum_{j=1, j \neq k}^d r_j r_{j+1} \right)$ ; 2) compute the sparse tensor  $\mathcal{S}$ , requiring  $2|\Omega| r_1 r_2$  flops; 3) compute the Euclidean gradient by sparse-dense matrix product which involves  $2|\Omega| \bar{r}$  flops, where  $\bar{r} := \sum_{k=1}^d r_k r_{k+1}$ ; 4) compute  $\mathbf{H}_k(\vec{\mathbf{W}})$  by a dense-dense matrix multiplication with  $2 \sum_{k=1}^d n_{-k} (r_k r_{k+1})^2$  flops; 5) compute the Riemannian gradient through Cholesky decomposition for linear systems, which requires  $\sum_{k=1}^d (2n_k (r_k r_{k+1})^2 + C_{\text{chol}} (r_k r_{k+1})^3)$  flops. Following above operations, the straightforward computation of the Riemannian gradient totally requires  $2|\Omega| r_1 r_2 + 2|\Omega| d \bar{r} + \sum_{k=1}^d (2n_{-k} R_k + 2n_{-k} (r_k r_{k+1})^2 + 2n_k (r_k r_{k+1})^2 + C_{\text{chol}} (r_k r_{k+1})^3)$  flops. If  $n_1 = \dots = n_d = n$  and  $r_1 = \dots = r_d = r$ , it boils down to

$$2(d+1)|\Omega|r^2 + 2d(d-1)n^{d-1}r^3 + 2dn^{d-1}r^4 + 2dnr^4 + C_{\text{chol}}dr^6$$

flops in total. In practice, the terms with order of  $\mathcal{O}(n^{d-1})$  dominate the computational cost.

By using the Kronecker product structure of  $\mathbf{W}_{\neq k}^\top \mathbf{W}_{\neq k}$ , the total cost can be significantly reduced. [Algorithm 3.3](#) illustrates how to compute  $\mathbf{W}_{\neq k}^\top \mathbf{W}_{\neq k}$  without forming  $\mathbf{W}_{\neq k}$  explicitly.

The matrix multiplication is

$$(3.10) \quad \mathbf{W}_{\neq k}^\top \mathbf{W}_{\neq k} = \sum_{i=1}^{n-k} \mathbf{W}_{\neq k}(\cdot, i) \mathbf{W}_{\neq k}(\cdot, i)^\top = \sum_{\mathbf{i}_{-k}} \tilde{\mathbf{w}}_k(\mathbf{i}_{-k}) \tilde{\mathbf{w}}_k(\mathbf{i}_{-k})^\top,$$

where  $\tilde{\mathbf{w}}_k(\mathbf{i}_{-k}) := \text{vec}(\left(\prod_{j=k+1}^d \mathbf{U}_j(i_j) \prod_{j=1}^{k-1} \mathbf{U}_j(i_j)\right)^\top)$  and  $\mathbf{i}_{-k} := (i_{k+1}, \dots, i_d, i_1, \dots, i_{k-1}) \in [n_{k+1}] \times \dots \times [n_d] \times [n_1] \times \dots \times [n_{k-1}]$ . By using  $\text{vec}(\mathbf{C}\mathbf{X}\mathbf{B}^\top) = (\mathbf{B} \otimes \mathbf{C}) \text{vec}(\mathbf{X})$  for matrices  $\mathbf{B}, \mathbf{C}, \mathbf{X}$  in appropriate size, we have

$$(3.11) \quad \begin{aligned} \tilde{\mathbf{w}}_k(\mathbf{i}_{-k}) &= \left( (\mathbf{U}_{k+1}(i_{k+1}) \cdots \mathbf{U}_d(i_d) \mathbf{U}_1(i_1) \cdots \mathbf{U}_{k-1}(i_{k-1})) \otimes \mathbf{I}_{r_k} \right) \text{vec}(\mathbf{U}_{k-1}(i_{k-1})^\top) \\ &= \prod_{j=k+1}^d (\mathbf{U}_j(i_j) \otimes \mathbf{I}_{r_k}) \prod_{j=1}^{k-1} (\mathbf{U}_j(i_j) \otimes \mathbf{I}_{r_k}) \text{vec}(\mathbf{U}_{k-1}(i_{k-1})^\top), \end{aligned}$$

where  $\otimes$  denotes the Kronecker product. Taking (3.11) into (3.10), we can compute  $\mathbf{W}_{\neq k}^\top \mathbf{W}_{\neq k}$  in a recursive way,

$$\begin{aligned} \tilde{\mathbf{H}}_1 &:= \sum_{i_{k-1}=1}^{n_{k-1}} \text{vec}(\mathbf{U}_{k-1}(i_{k-1})^\top) \text{vec}(\mathbf{U}_{k-1}(i_{k-1})^\top)^\top, \\ \tilde{\mathbf{H}}_2 &:= \sum_{i_{k-2}=1}^{n_{k-2}} (\mathbf{U}_{k-2}(i_{k-2}) \otimes \mathbf{I}_{r_k}) \tilde{\mathbf{H}}_1 (\mathbf{U}_{k-2}(i_{k-2})^\top \otimes \mathbf{I}_{r_k}), \\ &\vdots \\ \tilde{\mathbf{H}}_{d-1} &:= \sum_{i_{k+1}=1}^{n_{k+1}} (\mathbf{U}_{k+1}(i_{k+1}) \otimes \mathbf{I}_{r_k}) \tilde{\mathbf{H}}_{d-2} (\mathbf{U}_{k+1}(i_{k+1})^\top \otimes \mathbf{I}_{r_k}). \end{aligned}$$

It follows that  $\mathbf{W}_{\neq k}^\top \mathbf{W}_{\neq k} = \tilde{\mathbf{H}}_{d-1}$ . The computation of  $\mathbf{W}_{\neq 1}^\top \mathbf{W}_{\neq 1}, \dots, \mathbf{W}_{\neq d}^\top \mathbf{W}_{\neq d}$  requires  $\sum_{k=1}^d \left( 2n_{k-1}(r_k r_{k-1})^2 + 2 \sum_{i=1, i \neq k, k-1}^d n_i r_k^2 r_i r_{i+1} (r_i + r_{i+1}) \right)$  flops in [Algorithm 3.3](#). If  $n_1 = \dots = n_d$  and  $r_1 = \dots = r_d$ , computing the Riemannian gradient requires

$$2d(d-1)|\Omega|r^3 + 2|\Omega|r^2 + 4d(d-2)nr^5 + 2dnr^4 + C_{\text{chol}}dr^6$$

flops in total, which has the terms with order of  $\mathcal{O}(n)$ . In order to verify the improvement of [Algorithm 3.3](#), we report a numerical comparison on a real dataset in [Appendix A](#).

---

**Algorithm 3.3** Efficient computation of  $\mathbf{W}_{\neq k}^\top \mathbf{W}_{\neq k}$

---

**Input:**  $k \in [d]$ , core tensors  $\mathcal{U}_l = \text{ten}_{(2)}(\mathbf{W}_l)$ , slice matrices  $\mathbf{U}_l(i_l)$ ,  $i_l = 1, \dots, n_l$ ,  $l = 1, \dots, d$ .

- 1: Set  $j = \text{mod}(k - 2 + d, d) + 1$ .
- 2: Compute  $\tilde{\mathbf{H}}_1 = \sum_{i_j=1}^{n_j} \text{vec}(\mathbf{U}_j(i_j)^\top) \text{vec}(\mathbf{U}_j(i_j)^\top)^\top$ .
- 3: **for**  $l = 2, 3, \dots, d - 1$  **do**
- 4:   Set  $j = \text{mod}(k - l - 1 + d, d) + 1$ .
- 5:   Compute  $\tilde{\mathbf{H}}_l = \sum_{i_j=1}^{n_j} (\mathbf{U}_j(i_j) \otimes \mathbf{I}_{r_k}) \tilde{\mathbf{H}}_{l-1} (\mathbf{U}_j(i_j)^\top \otimes \mathbf{I}_{r_k})$ .
- 6: **end for**

**Output:**  $\tilde{\mathbf{H}}_{d-1} = \mathbf{W}_{\neq k}^\top \mathbf{W}_{\neq k}$ .

---

**4. Convergence Analysis.** The global convergence of TR-RGD and TR-RCG is analyzed in this section. Let  $\{\vec{\mathbf{W}}^{(t)}\}_{t \geq 0}$  be an infinite sequence generated by [Algorithm 3.1](#) or [Algorithm 3.2](#). We prove that every accumulation point of  $\{\vec{\mathbf{W}}^{(t)}\}_{t \geq 0}$  is a stationary point; see [Theorems 4.2](#) and [4.3](#).

**Lemma 4.1** ([\[7, Lemma 2.7\]](#)). *Let  $\mathcal{M}' \subseteq \mathcal{M}$  be a compact Riemannian submanifold. Let  $\mathcal{R}_x : \mathbb{T}_x \mathcal{M}' \rightarrow \mathcal{M}'$  be retraction.  $f : \mathcal{M}' \rightarrow \mathbb{R}$  has Lipschitz continuous gradient on the convex hull of  $\mathcal{M}'$ . Then, there exists a constant  $L > 0$ , such that*

$$|f(\mathcal{R}_x(\xi)) - f(x) - g_x(\xi, \text{grad}f(x))| \leq \frac{L}{2} g_x(\xi, \xi) \quad \text{for all } x \in \mathcal{M}', \xi \in \mathbb{T}_x \mathcal{M}'.$$

We observe the coercivity of  $f$  in [\(2.2\)](#) from the regularization term  $\frac{\lambda}{2} \|\vec{\mathbf{W}}\|_{\mathbb{F}}^2$ . Hence, the level set  $\mathcal{L} := \{\vec{\mathbf{W}} : f(\vec{\mathbf{W}}) \leq f(\vec{\mathbf{W}}^{(0)})\}$  is compact. The sequence of function values  $\{f(\vec{\mathbf{W}}^{(t)})\}_{t \geq 0}$ , obtained from [\(3.6\)](#) and [\(3.7\)](#), is monotonically decreasing. It follows that  $\{\vec{\mathbf{W}}^{(t)}\}_{t \geq 0}$  is a bounded sequence in  $\mathcal{L}$  with

$$\|\vec{\mathbf{W}}^{(t)}\|_{\mathbb{F}}^2 = \frac{2(f(\vec{\mathbf{W}}^{(t)}) - f_{\Omega}(\vec{\mathbf{W}}^{(t)}))}{\lambda} \leq \frac{2f(\vec{\mathbf{W}}^{(t)})}{\lambda} \leq \frac{2f(\vec{\mathbf{W}}^{(0)})}{\lambda}.$$

Therefore, there exist accumulation points for the sequence  $\{\vec{\mathbf{W}}^{(t)}\}_{t \geq 0}$ . Moreover, note that the objective function  $f$  has Lipschitz continuous gradient and the retraction on  $\mathbb{T}_{\vec{\mathbf{W}}} \mathcal{M}$  is the identity map. By using [Lemma 4.1](#) and [\[12, Proposition 4.3\]](#), we can prove the global convergence of the proposed Riemannian gradient descent algorithm in a same fashion.

**Theorem 4.2.** *Let  $\{\vec{\mathbf{W}}^{(t)}\}_{t \geq 0}$  be an infinite sequence generated by [Algorithm 3.1](#). Then, there exists  $C > 0$  such that  $f(\vec{\mathbf{W}}^{(t)}) - f(\vec{\mathbf{W}}^{(t+1)}) > C \|\text{grad}f(\vec{\mathbf{W}}^{(t)})\|_{\vec{\mathbf{W}}^{(t)}}$ . Furthermore, we have: 1) every accumulation point of  $\{\vec{\mathbf{W}}^{(t)}\}_{t \geq 0}$  is a stationary point of  $f$ ; 2) the algorithm returns  $\vec{\mathbf{W}} \in \mathcal{M}$  satisfying  $\|\text{grad}f(\vec{\mathbf{W}})\|_{\vec{\mathbf{W}}} < \epsilon$  after  $\lceil f(\vec{\mathbf{W}}^{(0)})/(C\epsilon^2) \rceil$  iterations at most.*

Now, we discuss the global convergence of the proposed Riemannian conjugate gradient algorithm in [Algorithm 3.2](#); interested readers are referred to [\[1, 28\]](#) for the convergence of RCG on general manifolds. Here, we follow the convergence analysis in [\[1\]](#). To fulfill the basic assumptions in [\[1, Theorem 4.3.1\]](#), i.e., the sequence of search directions  $\{\vec{\eta}^{(t)}\}_{t \geq 0}$  is gradient-related to  $\{\vec{\mathbf{W}}^{(t)}\}_{t \geq 0}$ , we enforce  $\vec{\eta}^{(t)}$  to be

$$(4.1) \quad \vec{\eta}^{(t)} = -\text{grad}f(\vec{\mathbf{W}}^{(t)}) \quad \text{if } g_{\vec{\mathbf{W}}^{(t)}}(\vec{\eta}^{(t-1)}, \text{grad}f(\vec{\mathbf{W}}^{(t)})) \geq 0.$$

Therefore,  $\{\vec{\eta}^{(t)}\}_{t \geq 0}$  are descent directions with

$$(4.2) \quad \begin{aligned} g_{\vec{\mathbf{W}}^{(t)}}(\vec{\eta}^{(t)}, \text{grad}f(\vec{\mathbf{W}}^{(t)})) &= -\|\text{grad}f(\vec{\mathbf{W}}^{(t)})\|_{\vec{\mathbf{W}}^{(t)}}^2 + \beta^{(t)} g_{\vec{\mathbf{W}}^{(t)}}(\vec{\eta}^{(t-1)}, \text{grad}f(\vec{\mathbf{W}}^{(t)})) \\ &\leq -\|\text{grad}f(\vec{\mathbf{W}}^{(t)})\|_{\vec{\mathbf{W}}^{(t)}}^2. \end{aligned}$$

In addition, it follows from [Algorithm 3.2](#) that

$$(4.3) \quad \|\vec{\eta}^{(t)}\|_{\mathbb{F}} = \frac{\|\vec{\mathbf{W}}^{(t+1)} - \vec{\mathbf{W}}^{(t)}\|_{\mathbb{F}}}{s^{(t)}} \leq \frac{\|\vec{\mathbf{W}}^{(t+1)}\|_{\mathbb{F}} + \|\vec{\mathbf{W}}^{(t)}\|_{\mathbb{F}}}{s_{\min}} \leq \frac{2}{s_{\min}} \sqrt{\frac{2f(\vec{\mathbf{W}}^{(0)})}{\lambda}}$$

is uniformly bounded. In view of (4.2) and (4.3),  $\{\vec{\eta}^{(t)}\}_{t \geq 0}$  is gradient-related to  $\{\vec{\mathbf{W}}^{(t)}\}_{t \geq 0}$ . By using [1, Theorem 4.3.1], we have the following result.

**Theorem 4.3.** *Let  $\{\vec{\mathbf{W}}^{(t)}\}_{t \geq 0}$  be an infinite sequence generated by Algorithm 3.2 with modified search direction (4.1). Then, every accumulation point of  $\{\vec{\mathbf{W}}^{(t)}\}_{t \geq 0}$  is a stationary point of  $f$ .*

**5. Numerical Experiments.** In this section, we numerically compare TR-RGD (Algorithm 3.1) and TR-RCG (Algorithm 3.2) with existing algorithms based on different tensor decompositions on synthetic and real-world datasets, including movie ratings, hyperspectral images, and high-dimensional functions. First, we introduce all the compared algorithms and default settings.

We consider the Riemannian conjugate gradient algorithm<sup>1</sup> in [32] based on tensor train decomposition, which is denoted by “TT-RCG”. For CP-based algorithm, we choose “CP-WOPT” [2] in Tensor-Toolbox<sup>2</sup> by Bader and Kolda [4] with limited-memory BFGS algorithm<sup>3</sup> recommended by the authors. “GeomCG” [23] is a Riemannian conjugate gradient algorithm<sup>4</sup> for Tucker-based tensor completion problem. In addition, we consider a nuclear-norm-based algorithm<sup>5</sup> “HaLRTC” [24, 30]. If not specified, we adopt default settings for all the compared algorithm.

Note that there are different ways to choose stepsize. In the preliminary numerical experiments, TR-RGD with stepsize RBB2 in (3.8) performs better than the algorithm with RBB1. Therefore, we only consider stepsize RBB2 in the following comparisons. “TR-RGD (exact)” and “TR-RGD (RBB)” denote Algorithm 3.1 with exact line search (3.6) and Algorithm 3.1 with Armijo backtracking (3.7) and RBB2, respectively. Moreover, the vanilla Euclidean gradient descent algorithm, denoted by “TR-GD”, is implemented for comparison. The stepsize for TR-GD is based on Armijo backtracking and the standard BB [5]. The default settings of line search parameters are  $\rho = 0.4$ ,  $a = 10^{-5}$ , and  $s_{\min} = 10^{-10}$ . In addition, we implement the alternating least squares algorithm [34, 36] called “TR-ALS” for the tensor completion problem (2.2).

All algorithms are initialized from  $\mathcal{X}^{(0)} = \tau(\vec{\mathbf{W}})$  in which  $\tau$  is defined in (2.3) and  $\vec{\mathbf{W}}$  is randomly generated. We define the relative error on a sampling set  $\Omega$

$$\varepsilon_{\Omega}(\vec{\mathbf{W}}) := \frac{\|P_{\Omega}(\tau(\vec{\mathbf{W}})) - P_{\Omega}(\mathcal{A})\|_{\text{F}}}{\|P_{\Omega}(\mathcal{A})\|_{\text{F}}}.$$

We refer to the training error as  $\varepsilon_{\Omega}(\vec{\mathbf{W}})$ . Furthermore, we evaluate the test error  $\varepsilon_{\Gamma}(\vec{\mathbf{W}})$  on a test set  $\Gamma$  different from  $\Omega$ . The default setting of  $|\Gamma|$  is 100. For stopping criteria, we terminate the algorithms once one of the following criteria is reached: 1) the relative error  $\varepsilon_{\Omega} < 10^{-12}$ ; 2) the relative change  $|(\varepsilon_{\Omega}(\vec{\mathbf{W}}^{(t)}) - \varepsilon_{\Omega}(\vec{\mathbf{W}}^{(t-1)})) / \varepsilon_{\Omega}(\vec{\mathbf{W}}^{(t-1)})| < \varepsilon$ ; 3) the gradient norm  $\|\text{grad}f(\vec{\mathbf{W}})\|_{\text{F}} < \varepsilon$ ; 4) maximum iteration number; 5) time budget. The tolerance  $\varepsilon$  is

<sup>1</sup>TTeMPS toolbox: <https://www.epfl.ch/labs/anchp/index-html/software/ttemps/>.

<sup>2</sup>Tensor-Toolbox v3.4: <http://www.tensor toolbox.org/>.

<sup>3</sup>Available from <https://github.com/stephenbeckr/L-BFGS-B-C>.

<sup>4</sup>GeomCG toolbox: <https://www.epfl.ch/labs/anchp/index-html/software/geomcg/>.

<sup>5</sup>Available from [https://github.com/andrewssobral/mctc4bmi/tree/master/alg\\_s\\_tc/LRTC](https://github.com/andrewssobral/mctc4bmi/tree/master/alg_s_tc/LRTC).

chosen as  $10^{-8}$ . All experiments are performed on a MacBook Pro 2019 with MacOS Ventura 13.1, 2.4 GHz 8 core Intel Core i9 processor, 32GB memory, and Matlab R2020b.

**5.1. Synthetic data.** In this subsection, we investigate the numerical performance and the reconstruction ability of tensor completion algorithms in TR decomposition on noiseless and noisy observations.

*Noiseless observations.* We consider a synthetic low-rank tensor  $\mathcal{A} \in \mathbb{R}^{n_1 \times \dots \times n_d}$  in (2.2) generated by

$$\mathcal{A} = \tau(\vec{\mathbf{W}}),$$

where  $\tau$  is defined in (2.3), each entry of  $\vec{\mathbf{W}} \in \mathcal{M}$  is uniformly sampled from  $[0, 1]$ ,  $d = 3$ ,  $n_1 = n_2 = n_3 = 100$ , and TR rank  $\mathbf{r}^* = (6, 6, 6)$ . Given the sampling rate  $p$ , we formulate the sampling set  $\Omega$  by randomly selecting  $pn_1 \dots n_d$  samples from  $[n_1] \times \dots \times [n_d]$ . In order to get an unbiased recovery result, we choose the regularization parameter  $\lambda = 0$ , the sampling rate  $p = 0.3$ , and  $\mathbf{r} = (6, 6, 6)$ . The time budget is 1800s and the maximum iteration number is 10000.

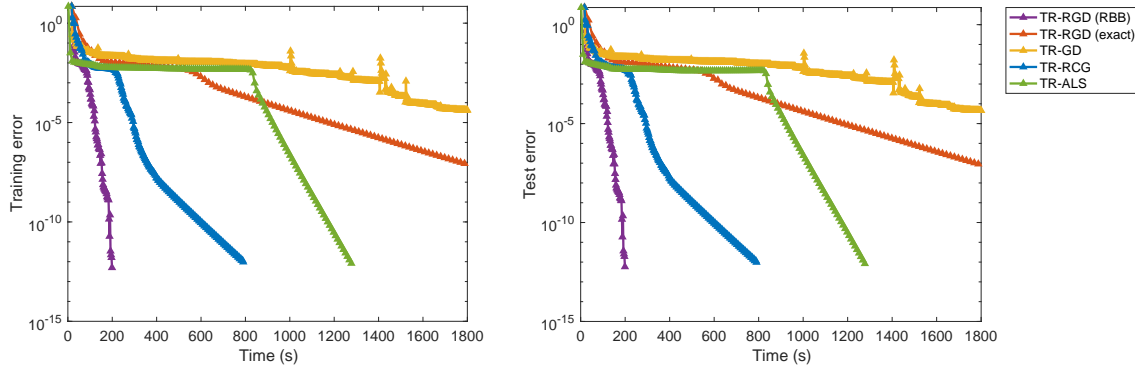


**Figure 2.** Numerical results of noiseless case. Left: training error. Right: test error.

Figure 2 presents the numerical results of noiseless case. First, we observe that the TR-RGD (RBB), TR-RCG, and TR-ALS algorithms successfully recover the true tensor within time budget. TR-RGD (RBB) and TR-RCG perform better than the alternating least squares algorithm (TR-ALS) in terms of training error and test error, and TR-RGD (RBB) is slightly better than TR-RCG. Second, TR-RGD with RBB stepsize is more efficient than the algorithm with exact line search, since computing exact line search needs to find the roots for a polynomial of degree  $2d - 1$ . However, computing the coefficients of such polynomial is expensive in practice. Third, it is worth noting that the proposed Riemannian gradient algorithms outperform the Euclidean gradient algorithm, implying that the new metric have a preconditioning effect indeed.

The question “how many samples are required to recover a low-rank data” is interesting but challenging. In the matrix case ( $d = 2$ ), around  $\mathcal{O}(nr \log n)$  samples are necessary to recover a low-rank matrix [20, 10]. In order to numerically investigate this question in low-rank tensors, we randomly generate the third order synthetic tensors  $\mathcal{A}$  with TR rank  $\mathbf{r} = (3, 3, 3)$  in the same fashion as above, and select tensor size  $n := n_1 = n_2 = n_3$  from  $\{60, 70, \dots, 180\}$

and the sample size  $|\Omega|$  from  $\{1000, 1500, \dots, 20000\}$ . We run TR-RGD, TR-RCG, and TR-ALS algorithms five times for each combination of  $n$  and  $|\Omega|$ . One algorithm is regarded to successfully recover a tensor if the test error  $\varepsilon_\Gamma < 10^{-4}$  within maximum iteration number 250. Figure 3 illustrates the phase plots of recovery results, in which the gray level of each block represents the number of successful recovery. White blocks imply successful recovery in all five runs. The red line represents  $\mathcal{O}(nr \log n)$  when  $n$  scales. The phase plots suggest a similar behavior to the matrix case, which is consistent to other numerical experiments for  $d = 3$ , e.g., [23]. In addition, we observe from Figure 3 that TR-RCG has more white blocks. Therefore, it reveals that TR-RCG is less sensitive to initial points.

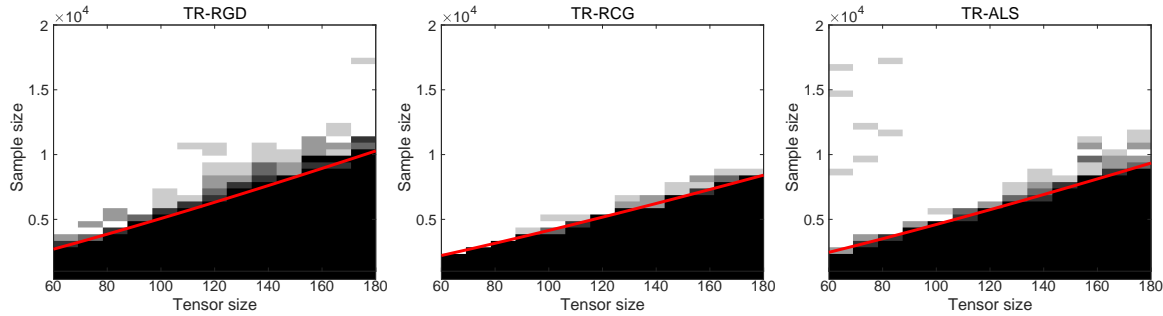


Figure 3. Phase plots of recovery results.

*Noisy observations.* Furthermore, we investigate the reconstruction ability of TR-based algorithms under different noise levels. We consider a synthetic noisy tensor

$$\mathcal{A} := \frac{\hat{\mathcal{A}}}{\|\hat{\mathcal{A}}\|_F} + \sigma \cdot \frac{\mathcal{E}}{\|\mathcal{E}\|_F},$$

where  $\hat{\mathcal{A}}$  is generated in the same rule as the noiseless case.  $\mathcal{E}$  is a tensor with its entries being sampled from normal distribution  $\mathcal{N}(0, 1)$ . The parameter  $\sigma$  measures the noise level of a tensor. Ideally, the relative errors  $\varepsilon_\Omega$  and  $\varepsilon_\Gamma$  are supposed to be the noise level  $\sigma$  when the algorithm terminates. We set  $\sigma = 10^{-3}, 10^{-4}, 10^{-5}, 10^{-6}, 10^{-7}, 10^{-8}$ , the regularization parameter  $\lambda = 10^{-10}$ , and the sampling rate  $p = 0.05$ . The time budget is 300s and the maximum iteration number is 300. Figure 4 shows the recovery performance of TR-based algorithms under different noise levels. All algorithms successfully recover the underlying low-rank tensor within time budget except TR-GD.

**5.2. Experiments on MovieLens 1M dataset.** We consider a real-world tensor completion problem on the MovieLens 1M<sup>6</sup> dataset including one million movie ratings from 6040 users on 3952 movies from September 19th, 1997 to April 22nd, 1998. We formulate the movie ratings as a third order tensor  $\mathcal{A}$  of size  $6040 \times 3952 \times 150$  by choosing one week as a period. We randomly select 80% of the known ratings as training set  $\Omega$  and the rest 20% ratings are test set  $\Gamma$ . We compared the proposed algorithms TR-RGD and TR-RCG with other tensor completion algorithms including TR-GD, TR-ALS, TT-RCG, CP-WOPT, and geomCG. We

<sup>6</sup>Available from <https://grouplens.org/datasets/movielens/1m/>.

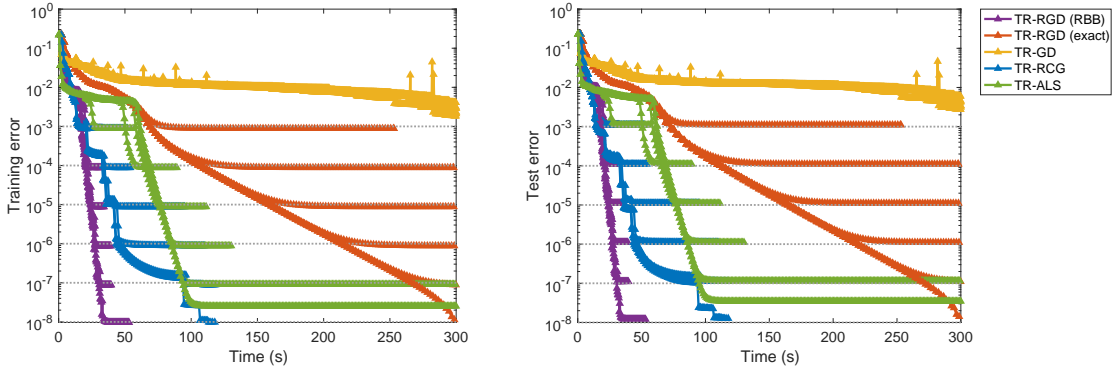


**Figure 4.** Reconstruction ability of TR-based algorithms under different noise levels. Left: training error. Right: test error.

choose the parameters: TR rank  $\mathbf{r} = (6, 10, 3)$  and  $\mathbf{r} = (6, 6, 6)$ , regularization parameter  $\lambda = 1$ , and the time budget 1000s. To ensure a close number of parameters in different search spaces, we choose the TT rank as  $(1, 10, 10, 1)$  and  $(1, 9, 9, 1)$ , the Tucker rank as  $(60, 30, 18)$  and  $(36, 36, 36)$ , and the CP rank as 49 and 36.

The test error under two different rank selections are shown in Figure 5. We observe that the proposed TR-RGD (RBB) and TR-RCG have faster convergence with lower test errors than the others, and the performance of TR-RGD (RBB) is comparable with TR-RCG in this scenario. Moreover, TR-RGD (exact) spends more time than TR-RGD (RBB). For the sake of brevity, we only consider TR-RGD (RBB) in the following experiments and simplify “TR-RGD (RBB)” to “TR-RGD”.

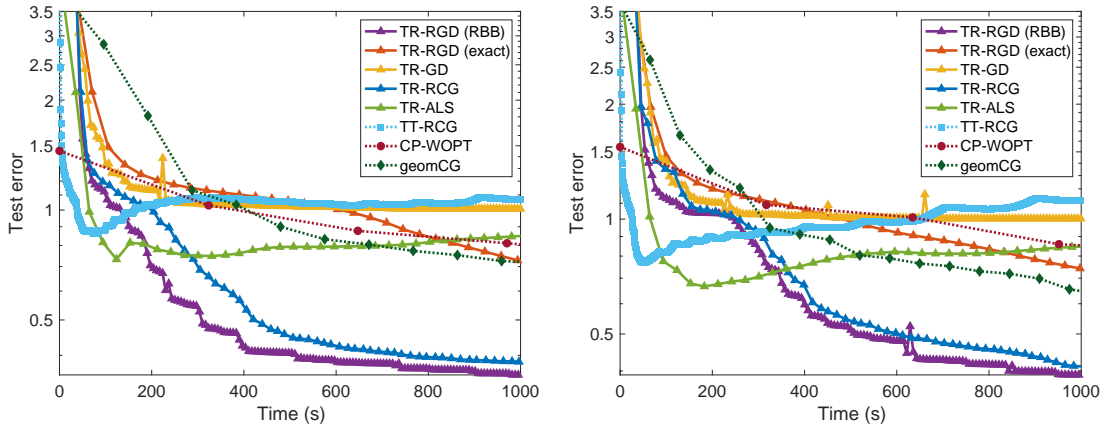


**Figure 5.** Test error on MovieLens 1M dataset. Left:  $\mathbf{r} = (6, 6, 6)$ . Right:  $\mathbf{r} = (6, 10, 3)$ .

**5.3. Experiments on hyperspectral images.** In this experiment, we consider the completion task on hyperspectral images. A hyperspectral image is formulated as a third order tensor  $\mathcal{A} \in \mathbb{R}^{n_1 \times n_2 \times n_3}$ . Mode three of  $\mathcal{A}$  represents  $n_3$  wavelength values of light. Mode one and

two represents reflectance level of light under different wavelengths. We select two images<sup>7</sup> from “50 reduced hyperspectral reflectance images” by Foster [13]: “Ribeira Houses Shrubs”, abbreviated as “Ribeira”, with size  $249 \times 330 \times 33$ ; and “Bom Jesus Bush”, abbreviated as “Bush”, with the size  $250 \times 330 \times 33$ . We transform hyperspectral images to RGB images by following the tutorial<sup>8</sup>. Figure 6 shows these two hyperspectral images represented as RGB images. To evaluate the recovery performance of image completion, peak signal-to-noise ratio (PSNR) is used to measure the similarity of two images, defined by

$$\text{PSNR} := 10 \log_{10} \left( \frac{\max(\mathcal{A})^2}{\text{MSE}} \right) = 10 \log_{10} \left( n_1 n_2 n_3 \frac{\max(\mathcal{A})^2}{\|\mathcal{X} - \mathcal{A}\|_F^2} \right),$$

where  $\max(\mathcal{A})$  denotes the highest pixel value of  $\mathcal{A}$ , and  $\text{MSE} := \|\mathcal{X} - \mathcal{A}\|_F^2 / (n_1 n_2 n_3)$  is the mean square error. The relative error

$$\text{relerr}(\mathcal{X}) := \frac{\|\mathcal{X} - \mathcal{A}\|_F}{\|\mathcal{A}\|_F}$$

is also reported. In our experiments, the PSNR between a recovered image and original image will be reported after being transformed into RGB images. Given sampling rate  $p$ , we formulate the sampling set  $\Omega$  in the same fashion as subsection 3.3. The initial guess  $\mathcal{X}^{(0)}$  is randomly generated with normal distribution  $\mathcal{N}(0, 1)$ . We set the TR rank as  $\mathbf{r} = (8, 20, 10)$ , the Tucker rank as  $(65, 65, 7)$  following [23], the TT rank as  $(1, 15, 15, 1)$ , and the CP rank as 177. It follows that the search spaces are of a similar size for different tensor formats. Moreover, the nuclear-norm-based algorithm, HaLRTC [24], is compared. The maximum iteration number is 200.



**Figure 6.** Hyperspectral images. Left: “Ribeira House Shrubs”. Right: “Bom Jesus Bush”.

Numerical results for the completion of two hyperspectral images are shown in Figure 7 and Table 1. One difficulty of recovering the “Ribeira” image is shrubs around the buildings, which triggers different recovery quality of different algorithms. The recovery quality

<sup>7</sup>Image source: hsi\_34.mat and hsi\_46.mat from [https://figshare.manchester.ac.uk/articles/dataset/Fifty\\_hyperspectral\\_reflectance\\_images\\_of\\_outdoor\\_scenes/14877285](https://figshare.manchester.ac.uk/articles/dataset/Fifty_hyperspectral_reflectance_images_of_outdoor_scenes/14877285).

<sup>8</sup>[https://personalpages.manchester.ac.uk/staff/david.foster/Tutorial\\_HSI2RGB/Tutorial\\_HSI2RGB.html](https://personalpages.manchester.ac.uk/staff/david.foster/Tutorial_HSI2RGB/Tutorial_HSI2RGB.html).

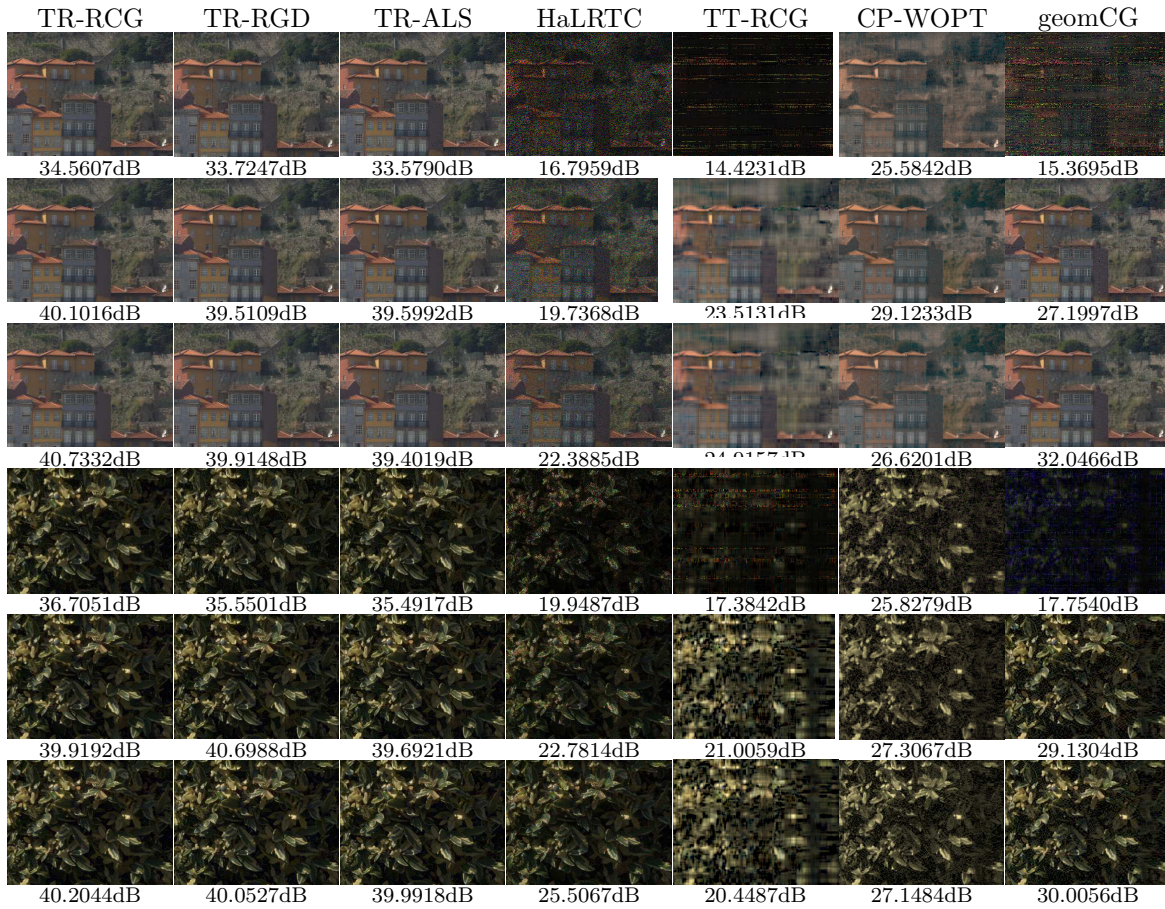


**Figure 7.** RGB representations of recovered images by different completion algorithms. The first three rows represent recovery results of the “Ribeira” image, under sampling rates  $p = 0.1, 0.3, 0.5$  in each row. The last three rows represent recovery results of the “Bush” image, under sampling rates  $p = 0.1, 0.3, 0.5$  in each row. The PSNR is displayed under each image.

of “Bush” image depends on the details of leaves. Figure 7 displays the recovery results under different sampling rates  $p = 0.1, 0.3, 0.5$ . The images recovered by TR-based algorithms (TR-RGD, TR-RCG, TR-ALS) depict more details than other candidates, e.g., the shrubs and the bushes. In fact, this observation can be quantified by the PSNR and relative errors; see Table 1. We observe that the proposed TR-RCG algorithm reaches the highest PSNR and the lowest relative error among all compared methods in most cases.

**5.4. Experiments on high-dimensional functions.** The discretization of high-dimensional functions  $h : [0, 1]^d \rightarrow \mathbb{R}$  requires storing a large tensor  $\mathcal{A} \in \mathbb{R}^{n_1 \times n_2 \times \dots \times n_d}$ , which is unfavorable in practice. To this end, one can apply tensor decomposition and tensor completion to recover the tensor  $\mathcal{A}$  by partially observed entries; see applications in [14]. In this subsection, we compare TR-based algorithms (TR-RGD, TR-RCG, TR-ALS) with TT-RCG on completion

Table 1

PSNR and relative errors for completion of two hyperspectral images, “Ribeira” and “Bush”.

Image	$p$	Results	TR-RCG	TR-RGD	TR-ALS	HaLRTC	TT-RCG	CP-WOPT	geomCG
Ribeira	0.1	PSNR(dB)	34.5607	33.7247	33.5790	16.7959	14.4231	25.5842	15.3695
		relerr	0.0954	0.1050	0.1068	0.7374	0.9710	0.2686	0.8691
	0.3	PSNR(dB)	40.1016	39.5109	39.5992	19.7368	23.5131	29.1233	27.1997
		relerr	0.0504	0.0539	0.0534	0.5256	0.3410	0.1787	0.2226
	0.5	PSNR(dB)	40.7322	39.9148	39.4019	22.3885	24.9157	26.6201	32.0466
		relerr	0.0469	0.0515	0.0546	0.3873	0.2901	0.2384	0.1274
Bush	0.1	PSNR(dB)	36.7051	35.5501	35.4917	19.9487	17.3842	25.8279	17.7540
		relerr	0.1066	0.1217	0.1225	0.7336	0.9855	0.3728	0.9444
	0.3	PSNR(dB)	39.9192	40.6988	39.6921	22.7814	21.0059	27.3067	29.1304
		relerr	0.0736	0.0673	0.0756	0.5294	0.6495	0.3144	0.2549
	0.5	PSNR(dB)	40.2044	40.0527	39.9918	25.5067	20.4487	27.1484	30.0056
		relerr	0.0712	0.0725	0.0730	0.3868	0.6925	0.3202	0.2305

of  $\mathcal{A}$  generated from  $h$  by evenly dividing the mode  $k$  of  $\mathcal{A}$  into  $n_k - 1$  intervals. Specifically,

$$\mathcal{A}(i_1, i_2, \dots, i_d) = h \left( \frac{i_1 - 1}{n_1 - 1}, \frac{i_2 - 1}{n_2 - 1}, \dots, \frac{i_d - 1}{n_d - 1} \right), \quad i_k = 1, \dots, n_k, \quad k = 1, \dots, d.$$

We consider the following two functions [32, §5.4.2],

$$h_1: [0, 1]^d \rightarrow \mathbb{R}, \quad h_1(\mathbf{x}) := \exp(-\|\mathbf{x}\|), \quad \text{and}$$

$$h_2: [0, 1]^d \rightarrow \mathbb{R}, \quad h_2(\mathbf{x}) := \frac{1}{\|\mathbf{x}\|},$$

We set  $d = 4$ ,  $n_1 = n_2 = n_3 = n_4 = 20$ , and the sampling rate  $p = 0.001, 0.005, 0.01, 0.05, 0.1$ . We follow the same way in subsection 5.1 to create the sampling set  $\Omega$ . The rank-increasing strategy is implemented to both TT and TR algorithms by following [32]. In order to choose a search space with similar size, we set the maximum rank of TT-RCG as  $(1, 5, 5, 5, 1)$ , and the maximum rank for TR-based algorithms as  $(4, 4, 4, 4)$ .

Table 2

Test errors for high-dimensional functions.

$p$	$h_1(\mathbf{x}) = \exp(-\ \mathbf{x}\ )$				$h_2(\mathbf{x}) = 1/\ \mathbf{x}\ $			
	TR-RGD	TR-RCG	TR-ALS	TT-RCG	TR-RGD	TR-RCG	TR-ALS	TT-RCG
0.001	8.0884e-2	7.4157e-2	7.4161e-2	1.3445e-1	1.7531e-1	1.8106e-1	1.8081e-1	2.6876e-1
0.005	7.3505e-3	8.7366e-3	9.2121e-3	1.5904e-2	3.4428e-2	2.9218e-2	3.2090e-2	1.2899e-1
0.01	6.2650e-3	9.7247e-4	1.8737e-3	4.1233e-3	2.5230e-2	1.7676e-2	1.8697e-2	3.4675e-2
0.05	3.8862e-4	1.5019e-4	1.8218e-4	2.2991e-4	3.8510e-3	3.6002e-3	5.2173e-3	3.5697e-3
0.1	1.2251e-4	5.9871e-5	6.8898e-5	8.2512e-5	7.7886e-4	2.9423e-4	6.0423e-4	7.4727e-4

The numerical results for recovering high-dimensional functions  $h_1$  and  $h_2$  are reported in Table 2. It illustrates that all algorithms have comparable performance. TR-based algorithms perform favorably comparable to TT-RCG. Among all TR-based algorithms, TR-RCG has a better performance in most experiments.

**6. Conclusion and perspectives.** We have developed Riemannian preconditioned algorithms for the tensor completion problem based on tensor ring decomposition. The preconditioning effect stems from a metric defined on the product space of matrices generated from the mode-2 unfolding of core tensors. However, the straightforward calculation of Riemannian gradient requires large matrix multiplications that are unaffordable in practice. To this end, we have proposed a procedure that efficiently computes the Riemannian gradient without forming large matrices explicitly. The proposed algorithms enjoy global convergence results. Numerical comparisons on both synthetic and real-world datasets present promising results.

Since the rank parameter has to be fixed a priori, we are interested in rank-adaptive strategies that may result in more accurate completion. In addition, investigating the quotient geometry of tensor ring decomposition is attractive.

**Appendix A. Speedup of efficient gradient computation.** In contrast with naive computation, [Algorithm 3.3](#) provides an efficient way to compute the gradients. [Table 3](#) reports the speedup results on MovieLens 1M dataset. “Naive” denotes the non-optimized implementation, i.e., explicitly forming  $\mathbf{W}_{\neq k}$  and large matrix multiplication. The results show that the proposed algorithm is of great potential to be applied in large-scale problems.

**Table 3**

*Speedup of efficient gradient computation on MovieLens 1M dataset.*

#iter	Time (seconds)		Avg. speedup	Relerr on $\Omega$ ( $\varepsilon_\Omega$ )		Relerr on $\Gamma$ ( $\varepsilon_\Gamma$ )	
	Naive	Proposed		Naive	Proposed	Naive	Proposed
1	266.6065	37.3207	-	3.6812	3.6812	3.6944	3.6944
21	5012.0138	185.8566	31.9479×	0.9222	0.9222	1.0362	1.0362
41	9796.2492	328.9951	32.6722×	0.6040	0.6040	0.7395	0.7395
61	14710.5989	471.6516	33.2557×	0.3749	0.3749	0.5253	0.5253
81	19524.0375	614.6125	33.3582×	0.3274	0.3274	0.4788	0.4788

## REFERENCES

- [1] P.-A. ABSIL, R. MAHONY, AND R. SEPULCHRE, *Optimization algorithms on matrix manifolds*, in *Optimization Algorithms on Matrix Manifolds*, Princeton University Press, 2009, <https://doi.org/10.1515/9781400830244>.
- [2] E. ACAR, D. M. DUNLAVY, T. G. KOLDA, AND M. MØRUP, *Scalable tensor factorizations for incomplete data*, *Chemometrics and Intelligent Laboratory Systems*, 106 (2011), pp. 41–56, <https://doi.org/10.1016/j.chemolab.2010.08.004>.
- [3] C. A. ANDERSSON AND R. BRO, *Improving the speed of multi-way algorithms: Part I. Tucker3*, *Chemometrics and Intelligent Laboratory Systems*, 42 (1998), pp. 93–103, [https://doi.org/https://doi.org/10.1016/S0169-7439\(98\)00010-0](https://doi.org/https://doi.org/10.1016/S0169-7439(98)00010-0).
- [4] B. W. BADER AND T. G. KOLDA, *Efficient MATLAB computations with sparse and factored tensors*, *SIAM Journal on Scientific Computing*, 30 (2008), pp. 205–231, <https://doi.org/10.1137/060676489>.
- [5] J. BARZILAI AND J. M. BORWEIN, *Two-point step size gradient methods*, *IMA J. Numer. Anal.*, 8 (1988), pp. 141–148, <https://doi.org/10.1093/imanum/8.1.141>.
- [6] N. BOUMAL, *An introduction to optimization on smooth manifolds*, Cambridge University Press, 2023, <https://doi.org/10.1017/9781009166164>, <https://www.nicolasboumal.net/book>.
- [7] N. BOUMAL, P.-A. ABSIL, AND C. CARTIS, *Global rates of convergence for nonconvex optimization on manifolds*, *IMA Journal of Numerical Analysis*, 39 (2019), pp. 1–33, <https://doi.org/10.1093/imanum/drx080>.

- [8] N. BOUMAL, B. MISHRA, P.-A. ABSIL, AND R. SEPULCHRE, *Manopt, a Matlab toolbox for optimization on manifolds*, The Journal of Machine Learning Research, 15 (2014), pp. 1455–1459, <http://jmlr.org/papers/v15/boumal14a.html>.
- [9] J.-F. CAI, W. HUANG, H. WANG, AND K. WEI, *Tensor completion via tensor train based low-rank quotient geometry under a preconditioned metric*, arXiv preprint arXiv:2209.04786, (2022), <https://arxiv.org/abs/2209.04786>.
- [10] E. J. CANDÈS AND T. TAO, *The power of convex relaxation: Near-optimal matrix completion*, IEEE Transactions on Information Theory, 56 (2010), pp. 2053–2080, <https://doi.org/10.1109/TIT.2010.2044061>.
- [11] Z. CHEN, Y. LI, AND J. LU, *Tensor ring decomposition: optimization landscape and one-loop convergence of alternating least squares*, SIAM Journal on Matrix Analysis and Applications, 41 (2020), pp. 1416–1442, <https://doi.org/10.1137/19M1270689>.
- [12] S. DONG, B. GAO, Y. GUAN, AND F. GLINEUR, *New Riemannian preconditioned algorithms for tensor completion via polyadic decomposition*, SIAM Journal on Matrix Analysis and Applications, 43 (2022), pp. 840–866, <https://doi.org/10.1137/21M1394734>.
- [13] D. H. FOSTER AND A. REEVES, *Colour constancy failures expected in colourful environments*, Proceedings of the Royal Society B, 289 (2022), p. 20212483, <https://doi.org/10.1098/rspb.2021.2483>.
- [14] K. GLAU, D. KRESSNER, AND F. STATTI, *Low-rank tensor approximation for Chebyshev interpolation in parametric option pricing*, SIAM Journal on Financial Mathematics, 11 (2020), pp. 897–927, <https://doi.org/10.1137/19M1244172>.
- [15] L. GRASEDYCK, M. KLUGE, AND S. KRÄMER, *Alternating directions fitting (ADF) of hierarchical low rank tensors*, Verlag nicht ermittelbar, 2013, <http://www.dfg-spp1324.de/download/preprints/preprint149.pdf>.
- [16] M. R. HESTENES AND E. STIEFEL, *Methods of conjugate gradients for solving linear systems*, Journal of research of the National Bureau of Standards, 49 (1952), p. 409, [https://nvlpubs.nist.gov/nistpubs/jres/049/jresv49n6p409\\_A1b.pdf](https://nvlpubs.nist.gov/nistpubs/jres/049/jresv49n6p409_A1b.pdf).
- [17] B. IANNAZZO AND M. PORCELLI, *The Riemannian Barzilai–Borwein method with nonmonotone line search and the matrix geometric mean computation*, IMA Journal of Numerical Analysis, 38 (2018), pp. 495–517, <https://doi.org/10.1093/imanum/drx015>.
- [18] P. JAIN AND S. OH, *Provable tensor factorization with missing data*, in Advances in Neural Information Processing Systems, Z. Ghahramani, M. Welling, C. Cortes, N. Lawrence, and K. Weinberger, eds., vol. 27, Curran Associates, Inc., 2014, <https://proceedings.neurips.cc/paper/2014/file/c15da1f2b5e5ed6e6837a3802f0d1593-Paper.pdf>.
- [19] H. KASAI AND B. MISHRA, *Low-rank tensor completion: a Riemannian manifold preconditioning approach*, in Proceedings of The 33rd International Conference on Machine Learning, M. F. Balcan and K. Q. Weinberger, eds., vol. 48 of Proceedings of Machine Learning Research, New York, New York, USA, 20–22 Jun 2016, PMLR, pp. 1012–1021, <https://proceedings.mlr.press/v48/kasai16.html>.
- [20] R. KESHAVAN, A. MONTANARI, AND S. OH, *Matrix completion from noisy entries*, Advances in neural information processing systems, 22 (2009), <https://proceedings.neurips.cc/paper/2009/hash/aa942ab2bfa6ebda4840e7360ce6e7ef-Abstract.html>.
- [21] Y. KHOO, J. LU, AND L. YING, *Efficient construction of tensor ring representations from sampling*, Multiscale Modeling & Simulation, 19 (2021), pp. 1261–1284, <https://doi.org/10.1137/17M1154382>.
- [22] T. G. KOLDA AND B. W. BADER, *Tensor decompositions and applications*, SIAM review, 51 (2009), pp. 455–500, <https://doi.org/10.1137/07070111X>.
- [23] D. KRESSNER, M. STEINLECHNER, AND B. VANDEREYCKEN, *Low-rank tensor completion by Riemannian optimization*, BIT Numerical Mathematics, 54 (2014), pp. 447–468, <https://doi.org/10.1007/s10543-013-0455-z>.
- [24] J. LIU, P. MUSIALSKI, P. WONKA, AND J. YE, *Tensor completion for estimating missing values in visual data*, IEEE transactions on pattern analysis and machine intelligence, 35 (2012), pp. 208–220, <https://doi.org/10.1109/TPAMI.2012.39>.
- [25] B. MISHRA, K. A. APUROOP, AND R. SEPULCHRE, *A Riemannian geometry for low-rank matrix completion*, arXiv preprint arXiv:1211.1550, (2012), <https://arxiv.org/abs/1211.1550>.
- [26] I. OSELEDETS AND E. TYRTYSHNIKOV, *TT-cross approximation for multidimensional arrays*, Linear Algebra and its Applications, 432 (2010), pp. 70–88, <https://doi.org/10.1016/j.laa.2009.07.024>.

- [27] I. V. OSELEDETS, *Tensor-train decomposition*, SIAM Journal on Scientific Computing, 33 (2011), pp. 2295–2317, <https://doi.org/10.1137/090752286>.
- [28] H. SATO, *Riemannian conjugate gradient methods: General framework and specific algorithms with convergence analyses*, SIAM Journal on Optimization, 32 (2022), pp. 2690–2717, <https://doi.org/10.1137/21M1464178>.
- [29] U. SCHOLLWÖCK, *The density-matrix renormalization group in the age of matrix product states*, Annals of physics, 326 (2011), pp. 96–192, <https://doi.org/10.1016/j.aop.2010.09.012>.
- [30] A. SOBRAL AND E. ZAHZAH, *Matrix and tensor completion algorithms for background model initialization: A comparative evaluation*, Pattern Recognition Letters, (2016), <https://doi.org/10.1016/j.patrec.2016.12.019>.
- [31] N. SREBRO, J. RENNIE, AND T. JAAKKOLA, *Maximum-margin matrix factorization*, Advances in neural information processing systems, 17 (2004), <https://proceedings.neurips.cc/paper/2004/file/e0688d13958a19e087e123148555e4b4-Paper.pdf>.
- [32] M. STEINLECHNER, *Riemannian optimization for high-dimensional tensor completion*, SIAM Journal on Scientific Computing, 38 (2016), pp. S461–S484, <https://doi.org/10.1137/15M1010506>.
- [33] F. VERSTRAETE, V. MURG, AND J. I. CIRAC, *Matrix product states, projected entangled pair states, and variational renormalization group methods for quantum spin systems*, Advances in physics, 57 (2008), pp. 143–224, <https://doi.org/10.1080/14789940801912366>.
- [34] W. WANG, V. AGGARWAL, AND S. AERON, *Efficient low rank tensor ring completion*, in Proceedings of the IEEE International Conference on Computer Vision, 2017, pp. 5697–5705, <https://doi.org/10.1109/ICCV.2017.607>.
- [35] L. YUAN, J. CAO, X. ZHAO, Q. WU, AND Q. ZHAO, *Higher-dimension tensor completion via low-rank tensor ring decomposition*, in 2018 Asia-Pacific Signal and Information Processing Association Annual Summit and Conference (APSIPA ASC), IEEE, 2018, pp. 1071–1076, <https://doi.org/10.23919/APSIPA.2018.8659708>.
- [36] Q. ZHAO, M. SUGIYAMA, L. YUAN, AND A. CICHOCKI, *Learning efficient tensor representations with ring-structured networks*, in ICASSP 2019-2019 IEEE international conference on acoustics, speech and signal processing (ICASSP), IEEE, 2019, pp. 8608–8612, <https://doi.org/10.1109/ICASSP.2019.8682231>.
- [37] Q. ZHAO, G. ZHOU, S. XIE, L. ZHANG, AND A. CICHOCKI, *Tensor ring decomposition*, arXiv preprint arXiv:1606.05535, (2016), <https://arxiv.org/abs/1606.05535>.
- [38] X. ZHAO, M. BAI, D. SUN, AND L. ZHENG, *Robust tensor completion: Equivalent surrogates, error bounds, and algorithms*, SIAM Journal on Imaging Sciences, 15 (2022), pp. 625–669, <https://doi.org/10.1137/21M1429539>.